01 Feb 2010

Causal RLGC(ƒ) Models for Transmission Lines from Measured S-Parameters

Jianmin Zhang

James L. Drewniak
Missouri University of Science and Technology, drewniak@mst.edu

David Pommerenke
Missouri University of Science and Technology, davidjp@mst.edu

Marina Koledintseva
Missouri University of Science and Technology, marinak@mst.edu

et. al. For a complete list of authors, see https://scholarsmine.mst.edu/ele_comeng_facwork/917

Recommended Citation

J. Zhang et al., "Causal RLGC(ƒ) Models for Transmission Lines from Measured S-Parameters," *IEEE Transactions on Electromagnetic Compatibility*, vol. 52, no. 1, pp. 189-198, Institute of Electrical and Electronics Engineers (IEEE), Feb 2010.
The definitive version is available at https://doi.org/10.1109/TEMC.2009.2035055

Causal *RLGC*(f) Models for Transmission Lines From Measured S-Parameters

Jianmin Zhang, *Senior Member, IEEE*, James L. Drewniak, *Fellow, IEEE*, David J. Pommerenke, *Senior Member, IEEE*, Marina Y. Koledintseva, *Senior Member, IEEE*, Richard E. DuBroff, *Senior Member, IEEE*, Wheling Cheng, Zhiping Yang, *Senior Member, IEEE*, Qinghua B. Chen, *Member, IEEE*, and Antonio Orlandi, *Fellow, IEEE*

***Abstract*—Frequency-dependent causal *RLGC*(f) models are proposed for single-ended and coupled transmission lines. Dielectric loss, dielectric dispersion, and skin-effect loss are taken into account. The dielectric substrate is described by the two-term Debye frequency dependence, and the transmission line conductors are of finite conductivity. In this paper, three frequency-dependent *RLGC* models are studied. One is the known frequency-dependent analytical *RLGC* model (*RLGC*-I), the second is the *RLGC*(f) model (*RLGC*-II) proposed in this paper, and the third (*RLGC*-III) is same as the *RLGC*-II, but with causality enforced by the Hilbert transform in frequency domain. The causalities of the three *RLGC* models are corroborated in the time domain by examining the propagation of a well-defined pulse through three different transmission lines: a single-ended stripline, a single-ended microstrip line, and an edge-coupled differential stripline pair. A clear time-domain start point is shown on each received pulse for the *RLGC*-II model and the *RLGC*-III model, where their corresponding start points overlap. This indicates that the proposed *RLGC*(f) model (*RLGC*-II) is causal. Good agreement of simulated and measured S-parameters has also been achieved in the frequency domain for the three transmission lines by using the proposed frequency-dependent *RLGC*(f) model.**

***Index Terms*—Causality, dielectric materials, Hilbert transforms, scattering parameters, transmission line modeling.**

I. Introduction

Signal integrity analysis and channel modeling in high-speed digital systems are becoming more and more important as operating frequencies increase. When the on-board frequencies are above hundreds of megahertz, or especially in the gigahertz range, traces on printed circuit boards (PCBs) no longer behave as simple conductors, but exhibit high-frequency effects, and behave as transmission lines. Accurate models to simulate high-frequency effects, such as dielectric dispersion, skin-effect loss, and crosstalk, become critical, so it is desirable to obtain an accurate frequency-dependent causal *RLGC*(f) model to represent a transmission line. Though many cross-sectional static and quasi-static numerical tools are able to evaluate R, L, G, and C parameters for transmission lines, the condition is that the causal dielectric properties of the substrate materials must be known prior to using these tools. For accuracy, the R, L, G, and C parameters must be evaluated at different frequencies with different values of complex permittivity, which is cumbersome for a wide frequency range of interest. In addition, these cross-sectional tools are electrostatic field solvers in nature, and therefore, they may be suitable only for finding R, L, G, and C parameters at low frequencies, where quasi-static approximation is still valid, while accuracy at higher frequencies is lost. Furthermore, the frequency-dependent permittivity properties of a particular PCB substrate (typically, of flame retardant (FR)-4 type) are usually not known exactly. This is because dielectric properties for PCBs vary in a substantial range, depending on process technology and constituents contained in the substrates even for the same PCB manufacturer. To develop a frequency-dependent causal *RLGC*(f) model, not only both the dielectric loss and the conductor loss must be taken into account, but also the dielectric dispersion. However, it is very difficult or even impossible to find appropriate data in literature or in manufacturer's databases that could be applicable for describing a particular PCB in terms of dielectric frequency dispersion, e.g., using a Debye or a Lorentzian model [1]. If the dielectric dispersion is not taken into account and the dielectric is described by a constant real permittivity with a constant loss tangent, the dielectric response turns out to be noncausal. Indeed, real and imaginary parts of dielectric permittivity $\varepsilon(\omega)$ in any physically realizable linear dielectric medium are not independent of each other. They must satisfy the Kramers–Kronig relationships [2], which are analogous to Hilbert transforms for any passive linear filter [3], [4]

$$\begin{cases} \varepsilon_{\mathrm{real}}(\omega) = \dfrac{1}{\pi} P \displaystyle\int_{-\infty}^{\infty} \frac{\varepsilon_{\mathrm{imag}}(x)}{x-\omega} dx + 1 \\ \varepsilon_{\mathrm{imag}}(\omega) = -\dfrac{1}{\pi} P \displaystyle\int_{-\infty}^{\infty} \frac{\varepsilon_{\mathrm{real}}(x) - 1}{x-\omega} dx \end{cases} \tag{1}$$

where P denotes the Cauchy principal value that expands the class of functions for which the integral exists. As follows from (1), $\varepsilon_{\mathrm{real}}(\omega)$ can be determined from $\varepsilon_{\mathrm{imag}}(\omega)$ at any particular frequency if $\varepsilon_{\mathrm{imag}}(\omega)$ is known over the entire frequency range, or *vice versa*. Hence, an *RLGC* model of a transmission line can be causal only if the properties of the surrounding dielectrics have causal representations.

Manuscript received April 11, 2009; revised September 10, 2009. First published December 11, 2009; current version published February 18, 2010.

J. Zhang, Z. Yang, and Q. B. Chen are with Cisco Systems, Inc., San Jose, CA 95134 USA (e-mail: jianmin@cisco.com; zhiping@cisco.com; billchen@cisco.com).

J. L. Drewniak, D. J. Pommerenke, M. Y. Koledintseva, and R. E. DuBroff are with the Missouri University of Science and Technology (formerly University of Missouri-Rolla), Rolla, MO 65409 USA (e-mail: drewniak@mst.edu; davidjp@mst.edu; marina@mst.edu; red@mst.edu).

W. Cheng is with Juniper Networks, Sunnyvale, CA 94089 USA (e-mail: whelingcheng@gmail.com).

A. Orlandi is with the University of L'Aquila, L'Aquila, I-67010, Italy (e-mail: orlandi@ing.univaq.it).

Color versions of one or more of the figures in this paper are available online at http://ieeexplore.ieee.org.

Digital Object Identifier 10.1109/TEMC.2009.2035055

A lossy transmission line *RLGC* model was first proposed for coaxial cables, where there is no radiation loss. In the early studies of loss for transmission lines, only skin-effect loss was considered, while dielectric loss was neglected [5]. Wigington and Nahman [5] had shown that the simple skin-effect loss followed a $\sqrt{f}$ law, and later, Nahman [6] presented a transient model of a lossy cable by taking into account both the skin-effect loss and the dielectric loss. Nahman's representation of the dielectric loss was

$$G\left(f\right) = A f \varepsilon\left(f\right) \tag{2}$$

with a geometry-related constant A and frequency-dependent permittivity $\varepsilon(f)$. Nahman also theoretically discussed causal responses from the point of view of cable loss. However, no causal *RLGC* model was developed at that time. Instead, his interest was focused on a graphical transient analysis technique. In later studies [7], [8], Nahman and coworkers extended the skin-effect loss model to higher frequencies. Arabi *et al*. [9] improved the skin-effect loss model by adding a nonlinear phase term ($R_o/(2L\sqrt{f})$ versus 1) to the total phase in the transmission line propagation term $e^{-\gamma l}$ to take into account the phase effects due to the inductance variation of the transmission line at higher frequencies. In the aforementioned nonlinear phase term, R_o is the per-unit-length (p.u.l.) resistance determined by the transmission line structure and L is the transmission line p.u.l. inductance. No dielectric loss model was formulated in [9]. Svensson and Dermer developed a lossy *RLC* model, where both the dielectric loss and the skin-effect loss were taken into account [10]. A physical relaxation model used in their study to describe the dielectric loss is given by

$$\varepsilon = \varepsilon_1 + \int_{\tau 1}^{\tau 2} \frac{a/\tau}{1 + j\omega\tau} d\tau \tag{3}$$

where τ is the relaxation time, a is the "relaxation strength," and ε_1 is the dielectric permittivity without the contribution from relaxation term. The integrand in (3) is a Debye term [11], but after integration, permittivity is different from the Debye model. It is important to note that the parameters in the relaxation model are unknown, and it is not easy to find them. Since nominal geometrical dimensions in [10] were directly used for the skin-effect loss calculation, the accuracy of the developed lossy *RLC* model was limited by manufacturing tolerance, such as trace width, trace thickness, substrate dielectric thickness, as well as conductor surface roughness.

An analytical frequency-dependent *RLGC* model was introduced in the high-optimized simulation program with integrated circuit emphasis (HSPICE), where dielectric loss, conductor loss, and high-frequency phase shift due to inductance variation were taken into account [12]. This is the *RLGC*-I model mentioned in the Abstract. The dielectric loss and the conductor loss were modeled as

$$\begin{cases} G\left(f\right) = G_0 + f G_d \\ R\left(f\right) = R_0 + \sqrt{f}\left(1 + j\right) R_s \end{cases} \tag{4}$$

where R_o and R_s are the p.u.l. dc resistance and skin-effect resistance, respectively. In (4), G_o was used to model the shunt current due to free electrons in imperfect dielectrics, and the power loss due to the dielectric polarization and rotation of dipoles under an alternating field was modeled by G_d [13]. The p.u.l. capacitance of the *RLGC* model defined in [12] is constant over the entire frequency range of interest. Thus, the model given in [12] is noncausal. However, using the above-mentioned model, good agreement between measured and simulated S-parameters has been reported in [14], while causality has still remained a problem to be fixed.

In this paper, a frequency-dependent causal *RLGC*(f) model (*RLGC*-II) is proposed and detailed in Section II-A for single-ended transmission lines. Section II-B describes how to obtain the unknowns for this causal model from measured S-parameters using an optimization technique, genetic algorithm (GA), and how to enforce causality in a single-ended line *RLGC* model (*RLGC*-III). For a coupled transmission line, frequency-dependent causal *RLGC*(f) models including *RLGC*-II model and *RLGC*-III model (causality enforced) are presented Section II-C. Based on the above-mentioned models, three cases: 1) a single-ended stripline; 2) a single-ended microstrip line; and 3) an edge-coupled differential stripline, are studied in Section III. Time-domain causality examination and frequency-domain S-parameter comparison between the *RLGC* circuit simulations and the corresponding measurements are also presented in Section III. Conclusions are summarized in Section IV.

II. Model Development and Parameter Extraction

The causal *RLGC*(f) model (*RLGC*-II) proposed in this paper is derived from the analytical model given in [12] by using a causal dielectric representation to solve the noncausal phenomena. Parameters (unknowns) in the proposed model are found from measured S-parameters using a GA. In reality, the practical dimensions of a transmission line differ from its nominal dimensions due to manufacturing tolerances in PCB fabrication and due to the surface roughness. The latter impacts the surface resistance of the transmission line and can be taken into account as causing an equivalent decrease of nominal conductivity of transmission line conductors in the frequency range of interest. To account for these nonideal effects and improve the model accuracy, the known nominal conditions are used to estimate initial parameter ranges in the GA parameter search, instead of using them to directly calculate some of the unknowns. This is especially beneficial, when a model is developed from measurements (e. g., from the measured S-parameters), as those nonideal effects have already been incorporated in the measurements.

A. Frequency-Dependent Causal RLGC(f) Model and S-Parameter Representation for Single-Ended Transmission Lines

The lossy transmission line *RLGC* model based on [12] was developed in [14], and good agreement was obtained between simulated and measured S-parameters in the frequency domain. However, the noncausal phenomena have remained. As mentioned in Section I, the constant p.u.l. capacitance and the constant dielectric loss assumed in the model imply that the dielectric representation is noncausal. To fix the problem associated with the noncausal dielectric representation, the two-term

Debye model is used in the proposed causal *RLGC*(f) model

$$\varepsilon(\omega) = \left(\varepsilon_\infty + \frac{\varepsilon_{s1} - \varepsilon_\infty}{1 + j\omega\tau_1} + \frac{\varepsilon_{s2} - \varepsilon_\infty}{1 + j\omega\tau_2}\right)\varepsilon_0 \tag{5}$$

where ε_∞ is the high-frequency relative permittivity, ε_0 is the permittivity in free space, ε_{s1} and τ_1 are the static dielectric constant and the relaxation time constant of the first-term Debye components, while ε_{s2} and τ_2 correspond to the second Debye term. As reported in [15], the two-term Debye model can successfully describe dielectric properties for FR-4 dielectric substrates up to 20 GHz. By separating the real and the imaginary parts, (5) can be rewritten as

$$\begin{aligned}\varepsilon(\omega) &= \left(\varepsilon_\infty + \frac{\varepsilon_{s1} - \varepsilon_\infty}{1 + (\omega\tau_1)^2} + \frac{\varepsilon_{s2} - \varepsilon_\infty}{1 + (\omega\tau_2)^2}\right)\varepsilon_0 \\ &\quad - j\omega\left(\frac{(\varepsilon_{s1} - \varepsilon_\infty)\tau_1}{1 + (\omega\tau_1)^2} + \frac{(\varepsilon_{s2} - \varepsilon_\infty)\tau_2}{1 + (\omega\tau_2)^2}\right)\varepsilon_0 \\ &= \varepsilon^r_{\mathrm{real}}\varepsilon_0 - j\varepsilon^r_{\mathrm{imag}}\varepsilon_0 \end{aligned} \tag{6}$$

where

$$\begin{cases} \varepsilon^r_{\mathrm{real}} = \left(\varepsilon_\infty + \frac{\varepsilon_{s1} - \varepsilon_\infty}{1 + (\omega\tau_1)^2} + \frac{\varepsilon_{s2} - \varepsilon_\infty}{1 + (\omega\tau_2)^2}\right) \\ \varepsilon^r_{\mathrm{imag}} = \omega\left(\frac{(\varepsilon_{s1} - \varepsilon_\infty)\tau_1}{1 + (\omega\tau_1)^2} + \frac{(\varepsilon_{s2} - \varepsilon_\infty)\tau_2}{1 + (\omega\tau_2)^2}\right). \end{cases} \tag{7}$$

The frequency-dependent loss tangent is then calculated as a ratio of imaginary and real parts of the permittivity

$$\tan(\delta)_f = \frac{\varepsilon^r_{\mathrm{imag}}}{\varepsilon^r_{\mathrm{real}}}. \tag{8}$$

The frequency-dependent p.u.l. capacitance can then be evaluated using

$$C(f) = K_g \varepsilon^r_{\mathrm{real}} \varepsilon_{\mathrm{o}} \tag{9}$$

where K_g is a geometry-related constant. The p.u.l. shunt conductance due to the dielectric loss is calculated via

$$G(f) = G_0 + 2\pi f C \tan(\delta)_f \tag{10}$$

where G_o is the shunt conductance at dc due to free electrons in imperfect dielectrics. Substituting (8) and (9) into (10), the frequency-dependent p.u. l shunt conductance is rewritten as

$$G(f) = G_0 + 2\pi f K_g \varepsilon^r_{\mathrm{imag}} \varepsilon_0. \tag{11}$$

The p.u.l. inductance L_∞ of a transmission line at high frequencies depends on its cross-sectional geometry and permeability of the surrounding material. For a given transmission line, an assumption that the p.u.l. inductance L_∞ is constant at high frequencies is reasonable, since dielectric materials are nonmagnetic.

The frequency-dependent resistance of the conductor, approximated as in (4), seems reasonable, since good agreement between simulations using (4) and measured S-parameters was demonstrated in [14]. This approximation is inherited in the causal *RLGC*(f) model proposed here. Based on the earlier discussions, the p.u.l. parameters of the proposed *RLGC*(f) model are summarized as follows:

$$\begin{cases} R(f) = R_0 + \sqrt{f}(1 + j)R_s \\ L(f) = L_\infty \\ G(f) = G_0 + 2\pi f K_g \varepsilon^r_{\mathrm{imag}}\varepsilon_0 \\ C(f) = K_g \varepsilon^r_{\mathrm{real}}\varepsilon_0. \end{cases} \tag{12}$$

The imaginary part included in the frequency-dependent resistance term can be considered as an effective inductance using the following transform:

$$L'(f) = \frac{R_s}{2\pi\sqrt{f}}. \tag{13}$$

By adding (13) to the p.u.l. inductance $L(f)$ and subtracting it from the p.u.l. resistance $R(f)$, the proposed frequency-dependent causal *RLGC*(f) model is

$$\begin{cases} R(f) = R_0 + \sqrt{f}R_s \\ L(f) = L_\infty + R_s/\left(2\pi\sqrt{f}\right) \\ G(f) = G_0 + 2\pi f K_g \varepsilon^r_{\mathrm{imag}}\varepsilon_0 \\ C(f) = K_g \varepsilon^r_{\mathrm{real}}\varepsilon_0. \end{cases} \tag{14}$$

Causality of this model will be further examined.

The propagation constant for a piece of transmission line with the p.u.l. parameters given in (14) is [16]

$$\gamma = \sqrt{(R(f) + j2\pi f L(f))(G(f) + j2\pi f C(f))} \tag{15}$$

and the characteristic impedance of the line is [16]

$$Z_c = \sqrt{\frac{(R(f) + j2\pi f L(f))}{(G(f) + j2\pi f C(f))}}. \tag{16}$$

The ABCD matrix for a uniform transmission line piece with length l can be calculated as [17]

$$\mathrm{ABCD} = \begin{bmatrix} A & B \\ C & D \end{bmatrix} = \begin{bmatrix} \cosh(\gamma l) & Z_o \cdot \sinh(\gamma l) \\ \sinh(\gamma l)/Z_o & \cosh(\gamma l) \end{bmatrix}. \tag{17}$$

Finally, the S-parameters for a single-ended transmission line are obtained from the ABCD matrix as [16]

$$\begin{bmatrix} S_{11} & S_{12} \\ S_{21} & S_{22} \end{bmatrix} = \begin{bmatrix} \frac{A + B/Z_0 - CZ_0 - D}{A + B/Z_0 + CZ_0 + D} & \frac{2(AD - BC)}{A + B/Z_0 + CZ_0 + D} \\ \frac{2}{A + B/Z_0 + CZ_0 + D} & \frac{-A + B/Z_0 - CZ_0 + D}{A + B/Z_0 + CZ_0 + D} \end{bmatrix} \tag{18}$$

where Z_o is the reference impedance.

B. GA Implementation and Causality Enforcement for a Single-Ended Transmission Line

The frequency-dependent *RLGC*(f) model (14) is potentially causal. However, its further examination is necessary, because the $R(f)$ term in the model (12) is known to be approximate. In order to check the causal characteristics of the model, two different methods are used in the GA optimization for finding the model parameters. In the first approach, only measured

S-parameters are used as the objective data for the model parameter searching. In the second approach, in addition to the measured S-parameters used as objective data, the Hilbert transform is implemented on the minimum-phase part of the wave propagation term $e^{-\gamma l}$ to enforce the causality requirements during the parameter search. The causal feature of the proposed model can then be explored by comparing the wave propagation using the parameters from the two different approaches aforementioned. Since the first approach (model *RLGC*-II) is similar to the second one (model *RLGC*-III), except neglecting the causality requirement enforcement in *RLGC*-II, the GA implementation is then focused on the model *RLGC*-III in the further discussion.

As follows from (14), to build up a frequency-dependent causal *RLGC*(f) model for a single-ended transmission line, a set of unknowns must be obtained: R_o, R_s, L_∞, G_o, K_g, $\varepsilon^r_{\rm real}$, and $\varepsilon^r_{\rm imag}$. Equation (7) indicates that the $\varepsilon^r_{\rm real}$ and the $\varepsilon^r_{\rm imag}$ can be represented over the entire frequency span by the five parameters $\varepsilon_\infty, \varepsilon_{s1}, \tau_1, \varepsilon_{s2}$, and τ_2. The causal *RLGC*(f) model for a single-ended transmission line is then formulated as

$$RLGC\,(f) = \Psi\left(\varepsilon_\infty, \varepsilon_{s1}, \tau_1, \varepsilon_{s2}, \tau_2, R_0, R_s, L_\infty, G_0, K_g\right). \tag{19}$$

This is straightforward for striplines. However, for a microstrip transmission line, the dielectric represented by a two-term Debye model is not exactly the one that corresponds to the substrate material. Instead, it is an effective dielectric, where both the substrate material and free space have to be taken into account. The effective Debye model simplifies the problem and improves the accuracy of the p.u.l. parameters in solving microstrip transmission line problems, since the filling factor associated with the microstrip geometry configuration and derived from electrostatic fields is eliminated in the related formulation.

The search of ten unknowns in (19) becomes an optimization procedure. This is because the number of the equations of the S-parameters at different frequency points is much greater than the number of the unknowns. Since GAs are powerful, robust, and efficient in global searching and optimization due to their mechanics of natural selection and natural genetics [18], a GA code is developed to search the global optimum values for the ten unknowns [1]. To implement a GA for solving an optimization problem, the problem itself must be represented and formulated mathematically. For the ten unknowns, it is necessary to define ten initial parameter ranges, which a possible solution for each unknown correspondingly belongs to. The initial ranges are estimated based on the transmission line configurations including the cross-sectional geometry, the conductivity of the transmission line conductor, and the constituent parameters of the surrounding dielectric materials. These known conditions are not directly involved in some of calculations of the unknowns. They are, instead, only used to evaluate the initial parameter ranges for the ten unknowns, which differ from the skin-effect loss, directly calculated from the nominal dimensions. Therefore, the unknowns extracted from GA in the proposed model are accurate. This is because the measured S-parameters include all the nonideal effects, such as the surface roughness and the dimension deviations of the transmission line. The S-parameter differences between the evaluation and the measurement, and the differences between the causal propagation term $H_c(f_i)$ and the evaluated propagation term $H(f_i)$ are defined as an objective function, where the subscript letter "c" stands for causal

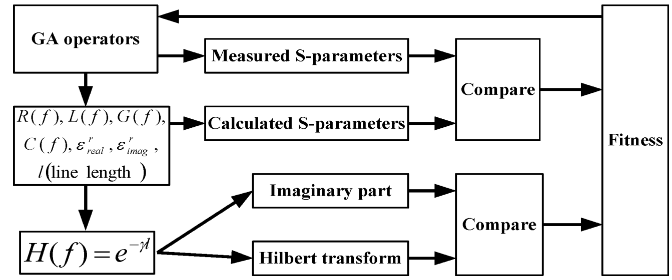

Fig. 1. GA flowchart of the parameter extraction for the *RLGC*(f) models.

$$\Delta = \frac{1}{N}\sqrt{\sum_{i=1}^{N}\left\{\begin{array}{l}\left[\frac{\left|\left|P_{21}^m(f_i)\right|-\left|P_{21}^e(f_i)\right|\right|}{\max\left|P_{21}^m\right|}\right]^2+\left[\frac{\left|\left|S_{21}^m(f_i)\right|-\left|S_{21}^e(f_i)\right|\right|}{\max\left|S_{21}^m\right|}\right]^2\\+\left[\frac{\left|\left|\mathrm{Im}(H(f_i))\right|-\left|\mathrm{Im}(H_c(f_i))\right|\right|}{\max\left|\mathrm{Im}(H_c(f_i))\right|}\right]^2\\+\left[\frac{\left|\left|\mathrm{Re}(H(f_i))\right|-\left|\mathrm{Re}(H_c(f_i))\right|\right|}{\max\left|\mathrm{Re}(H_c(f_i))\right|}\right]^2\end{array}\right\}} \tag{20}$$

where $|S^m_{21}\,(f_i)|$ and $|S^e_{21}\,(f_i)|$ are the magnitudes of the measured (index m) and evaluated (index e) S-parameters at frequency f_i, while $|P^m_{21}\,(f_i)|$ and $|P^e_{21}\,(f_i)|$ are the corresponding phases. The parameters $\max|S^m_{21}|$ and $\max|P^m_{21}|$ are the maximum absolute values over the entire frequency range of interest. Both propagation terms $H_c(f_i)$ and $H(f_i)$ are detailed later in this section. Re($H(f_i)$) and Re($H_c(f_i)$) are the real parts of $H(f_i)$ and $H_c(f_i)$, respectively, while Im($H(f_i)$) and Im($H_c(f_i)$) are the corresponding imaginary parts. The purpose of introducing $\max|S^m_{21}|$, $\max|P^m_{21}|$, $\max|\mathrm{Im}\,(H_c\,(f_i))|$, and $\max|\mathrm{Re}\,(H_c\,(f_i))|$ in (20) is to normalize the difference in each term so that Δ is unitless, and each term is equally weighted.

A fitness function, which is used to quantify the possible solution as "good" or "bad," is defined as [1]

$$p = \Delta^{-1/3}. \tag{21}$$

The higher the fitness index p, the more chance that the related value stays in the GA search pool as a parent to generate offspring for the next generation. Therefore, the fitness index is used for each possible solution to compete against the others in their solution space. The expected unknowns of the causal *RLGC*(f) model are obtained as Δ is minimized and p converges. A schematic program flowchart about the GA implementation is shown in Fig. 1. More general topics about GA operators, such as selection, recombination, and mutation, are described in [1] and [18]–[21], and they are beyond the interest of this paper.

The wave propagation term for a transmission line section with length l is [16]

$$H\,(\omega) = e^{-\gamma l} \tag{22}$$

where the propagation constant γ is defined based on the attenuation constant α and phase constant β as

$$\gamma = \alpha + j\beta. \tag{23}$$

Then the propagation term can be represented as

$$H(\omega) = e^{-\alpha l - j\beta l} = e^{-\theta(\omega) - j\varphi(\omega)} \tag{24}$$

where $\theta(\omega) = \alpha l$ and $\varphi(\omega) = \beta l$. In general, $\varphi(\omega)$ cannot be uniquely determined from $\theta(\omega)$ even if $H(\omega)$ is the transform of a causal function of $h(t)$ [22]. For the unique determination of $\varphi(\omega)$ from $\theta(\omega)$, it is necessary to impose certain conditions on the transfer function $H(\omega)$. According to linear system theory [23], any stable system function can be represented by the product of a minimum phase function $H_m(\omega)$ and an all-pass function $H_a(\omega)$ that has a unitary magnitude over the entire frequency span of interest as

$$H(\omega) = H_m(\omega)\, H_a(\omega). \tag{25}$$

There is the Bode condition for separating the transfer function $H(\omega)$ into a minimum phase function and an all-pass function, according to which the minimum phase function is defined as [6], [24]

$$\lim_{\omega\to\infty}\left(\frac{\gamma(\omega)}{j\omega}\right) \Rightarrow 0. \tag{26}$$

Substituting (7), (14), and (15) into (26), we get

$$\begin{aligned}\lim_{\omega\to\infty}\left(\frac{\gamma(\omega)}{j\omega}\right) &= \lim_{\omega\to\infty}\frac{1}{j}\sqrt{\begin{array}{c}\left(\frac{R(f)}{\omega} + j\left(L_\infty + \frac{R_s}{2\pi\sqrt{f}}\right)\right)\\ \left(\frac{G_o + K_g\,\omega\,\varepsilon^r_{\mathrm{imag}}\varepsilon_{\mathrm{o}}}{\omega} + jK_g\varepsilon^r_{\mathrm{real}}\varepsilon_{\mathrm{o}}\right)\end{array}}\\ &= \lim_{\omega\to\infty}\frac{1}{j}\sqrt{jL_\infty\left(K_g\varepsilon^r_{\mathrm{imag}}\varepsilon_{\mathrm{o}} + jK_g\varepsilon^r_{\mathrm{real}}\varepsilon_{\mathrm{o}}\right)}\\ &= \sqrt{L_\infty C_\infty}\end{aligned} \tag{27}$$

where $C_\infty$and L_∞ are the p.u.l. capacitance and inductance evaluated at infinite frequency. For a transmission line with the two-term Debye dielectric representation, the C_∞ corresponds to the "optical limit" dielectric constant ε_∞.

The relation shown in (27) indicates that a transmission line described by the *RLGC*(f) model (*RLGC*-II) is not a minimum-phase system in the general case. The causality can be enforced by removing the linear phase term $e^{-jl\sqrt{L_\infty C_\infty}}$ from the total phase. The transfer function (24) can then be rewritten as

$$H(\omega) = \left[e^{-\theta(\omega) - jP_m}\right] e^{-jl\sqrt{L_\infty C_\infty}} \tag{28}$$

where $P_m + l\sqrt{L_\infty C_\infty} = \varphi(\omega)$ and P_m is the minimum phase. By comparing (25) with (28), the all-pass function and the minimum-phase function is split as

$$\begin{cases} H_m(\omega) = e^{-\theta(\omega) - jP_m}\\ H_a(\omega) = e^{-jl\sqrt{L_\infty C_\infty}}.\end{cases} \tag{29}$$

The phase from the minimum phase function in (29) is then

$$\theta(\omega) + jP_m = -\ln\left(H_m(\omega)\right). \tag{30}$$

The real part and the imaginary part shown in (30) now meet the Kramers–Kronig relations, and the phase P_m can be uniquely determined from $\theta(\omega)$ by applying Hilbert transform, i.e.,

$$P_m = -\mathrm{Im}\left(\mathrm{Hilbert}\left(\theta(\omega)\right)\right) \tag{31}$$

where Im stands for the operation of obtaining the imaginary part after applying the Hilbert transform on $\theta(\omega)$. The phase $\theta(\omega)$ is

$$\theta(\omega) = -\ln\left|H(\omega)\right|. \tag{32}$$

Substituting (32) into (31), the phase P_m of the minimum phase function can then be restored from the natural logarithm of the magnitude of the transfer function (24) as

$$P_m = -\mathrm{Im}\left(\mathrm{Hilbert}\left(-\ln\left(\left|H(\omega)\right|\right)\right)\right). \tag{33}$$

The causal propagation term $H_c(\omega)$corresponding to the transmission line propagation term $H(\omega) = e^{-\gamma l}$ is built as

$$H_c(\omega) = \left|H(\omega)\right| e^{-jP_m}\, e^{-jl\sqrt{L_\infty C_\infty}}. \tag{34}$$

The GA objective function (20) and the fitness function (21) can be estimated based on both the causality requirements and the S-parameter differences between the measurements and the GA evaluations. The best solution (model parameters) is obtained for the *RLGC*(f) model as the causality requirements are met, and the S-parameter discrepancies are minimized.

C. Frequency-Dependent Causal RLGC(f) Model for Coupled Transmission Lines

The method to enforce the causality requirement in a coupled transmission line is more complicated than in a single-ended case. When compared with the single-ended model given in (19), two more unknowns must be added to the *RLGC*(f) model (*RLGC*-II) to take into account the coupling effects. One unknown is the p.u.l. mutual inductance L_m and the other is a geometry-related factor K_{gm}. The first unknown is associated with inductive coupling and the second one is related to capacitive coupling. The frequency-dependent causal *RLGC*(f) model for coupled transmission lines is then represented by 12 unknowns as

$$RLGC(f) = \Psi\begin{pmatrix}\varepsilon_\infty, \varepsilon_{s1}, \tau_1, \varepsilon_{s2}, \tau_2, R_0,\\ R_s, L_\infty, G_0, K_g, L_m, K_{gm}\end{pmatrix}. \tag{35}$$

The initial parameter range of the p.u.l. mutual inductance L_m can be evaluated from the initial parameter range of L_∞ as L_∞ and L_m are related by the coupling factor m as

$$m = \frac{L_m}{L_\infty} \tag{36}$$

where the two lines in the coupled differential stripline are assumed exactly same.

The initial parameter range for the geometry factor K_{gm} can be evaluated from the dimensions of the cross section of the coupled line. The p.u.l. mutual capacitance and the p.u.l. mutual shunt conductance of the transmission line can be evaluated as

$$C_m(f) = K_{gm}\varepsilon^r_{\mathrm{real}}\varepsilon_{\mathrm{o}} \tag{37}$$

$$G_{dm}(f) = 2\pi f K_{gm}\varepsilon^r_{\mathrm{imag}}\varepsilon_0. \tag{38}$$

To simplify the enforcement of the causality requirement in the coupled differential pair in the model *RLGC*-III, it is better to separate even and odd wave propagation modes along the transmission line. The propagation constants for the even mode γ_e and the odd mode γ_{odd} are calculated from

$$\gamma_e = \sqrt{(R(f) + j2\pi f L_e(f))(G_e(f) + j2\pi f C_e(f))} \quad (39)$$

$$\gamma_{\mathrm{odd}} = \sqrt{(R(f)+j2\pi f L_{\mathrm{odd}}(f))(G_{\mathrm{odd}}(f)+j2\pi f C_{\mathrm{odd}}(f))} \quad (40)$$

where $L_e, G_e, C_e, L_{\mathrm{odd}}, G_{\mathrm{odd}}$, and C_{odd} are evaluated from [17]

$$\begin{cases} L_e = L(f) + L_m \\ G_e = G(f) - G_{dm} \\ C_e = C(f) - C_m \end{cases} \quad (41)$$

$$\begin{cases} L_{\mathrm{odd}} = L(f) - L_m \\ G_{\mathrm{odd}} = G(f) + G_{dm} \\ C_{\mathrm{odd}} = C(f) + C_m. \end{cases} \quad (42)$$

The characteristic impedance for the even mode Z_e and the odd mode Z_{odd} can be calculated as

$$Z_e = \sqrt{\frac{(R(f) + j2\pi f L_e(f))}{(G_e(f) + j2\pi f C_e(f))}} \quad (43)$$

$$Z_{\mathrm{odd}} = \sqrt{\frac{(R(f) + j2\pi f L_{\mathrm{odd}}(f))}{(G_{\mathrm{odd}}(f) + j2\pi f C_{\mathrm{odd}}(f))}}. \quad (44)$$

The differential impedance and the common impedance is determined from

$$\begin{cases} Z_{\mathrm{com}} = 0.5 Z_e \\ Z_{\mathrm{dif}} = 2 Z_{\mathrm{odd}}. \end{cases} \quad (45)$$

For a coupled transmission line, the S-parameters can be easily evaluated for the common mode and the differential mode if the p.u.l. R, L, G, and C parameters of the *RLGC*(f) model and the transmission line length are known. While the S-parameters are under evaluation, the causality requirements have to be enforced for both even and odd modes. As long as the coupled problem is decomposed into even and odd modes, the earlier described procedure for single-ended transmission line can be directly used for solving coupled problems.

III. Case Studies

Three cases, a single-ended microstrip, a single-ended stripline, and an edge-coupled differential stripline, were studied based on the method described in Section II. All the S-parameters were measured using 8720ES VNA with ATN-4112 A S-parameters test set. The measurement frequency range was from 200 MHz to 20 GHz. "Thru-Reflect-Line" (TRL) calibration was used to remove the coaxial-connector-related port effects in the single-ended cases [16]. Two TRL calibration kits were designed and built on their corresponding test boards. The frequency span of each TRL calibration pattern was broken into three frequency ranges to meet the usable bandwidth for a single LINE/THRU (TRL calibration standards) pair less than 8:1 and the insertion phase in the range of 30°–150° [25]. For the coupled stripline, a new deembedding method was developed and used to eliminate the port effects [26].

The causality of a single-ended transmission line was tested using a well-defined time-domain pulse [27]

$$y(t) = \frac{10 (t/\tau_0)^n}{1 + (t/\tau_0)^n} e^{-t/\tau_0} \quad (46)$$

that was launched at one end (driving end) of the transmission line and observed at the other end (receiving end) with $\tau_0 =$ 0.1 ns and $n = 4$. Then *y(t)* was normalized to 1 by using $y(t)/\max(y(t))$. A MATLAB code was written to realize the observation. The time-domain pulse $y(t)$ launched at the driving end was converted into the frequency domain using a fast Fourier transform (FFT) to obtain its frequency-domain spectra. The propagation term $e^{-\gamma l}$ obtained from the *RLGC*(f) model was multiplied by the frequency spectra of $y(t)$, and the result was converted back to time domain using the inverse FFT (IFFT), i.e., FFT→IFFT procedure was done. For the coupled transmission line, the procedure was similar to the single-ended cases. But the coupled wave propagation was decomposed into even and odd modes, and the causality was examined for each mode separately.

To clearly show the causal/noncausal phenomena, each of the three studied transmission line cases was represented by three different *RLGC* models. The first model was the *RLGC*-I introduced in [12], and the model parameters were extracted using the method reported in [14]. The second method *RLGC*-II was the *RLGC*(f) model, proposed in this paper, where the ten (or 12) unknowns were obtained from the method described in Section II, with measured S-parameters as the only objective data. The third model *RLGC*-III was same as the *RLGC*-II, but with the enforced causality requirement, and hence, the parameters in these models could differ. The ten (or 12) unknowns of the third model (*RLGC*-III) were extracted using (20) as an objective function with causality requirements enforced in the model parameter extraction. Therefore, the causality in the *RLGC*-III model was guaranteed. Along with the causal/noncausal phenomenon observation, the S-parameters of each studied case were modeled by the three *RLGC*(f) representations. Comparisons of the obtained S-parameters and comparison of the time-domain waveforms at receiving end for the three studied cases were conducted.

The first studied case is a single-ended stripline. It is built on layer 7 within an eight-layer board having FR-4 as substrates. The cross-sectional dimensions of the stripline, the test board, and the measurement reference plane after TRL calibration are shown in Fig. 2. The thickness of the copper is $t =$ 1.35 mil, the width of the trace is $w =$ 12.5 mil, and the total height between the reference planes is $b =$ 27.7 mil. The stripline length after TRL calibration is 7976 mil. Fig. 3 demonstrates the comparison between the measured S-parameters, the corresponding results of HSPICE simulation using the *RLGC*-I model with the extracted model parameters, and the results of the *RLGC*(f) model with the parameters extracted using the abovementioned *RLGC*-II and *RLGC*-III methods. Comparison of the time-domain waveforms at the receiving end is shown in Fig. 4.

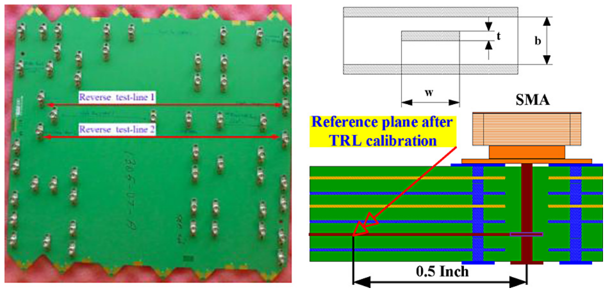

Fig. 2. Test board, TRL measurement reference plane, and cross-sectional dimensions of the single-ended stripline.

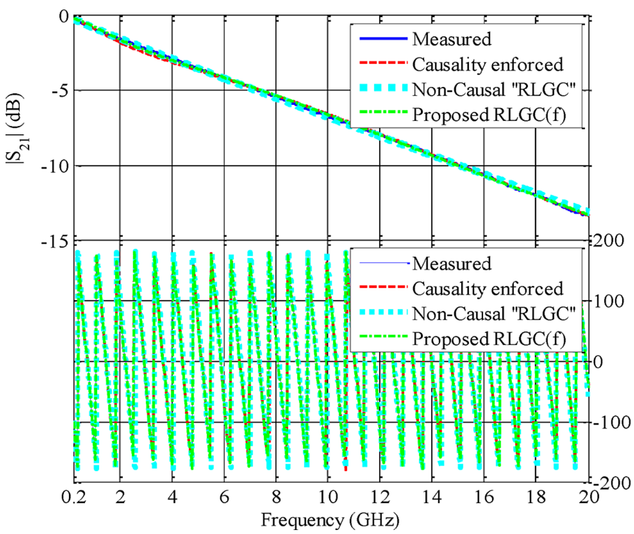

Fig. 3. S-parameter comparison between the *RLGC*(f) models (*RLGC*-I, II, and III) and the measurements for the single-ended stripline.

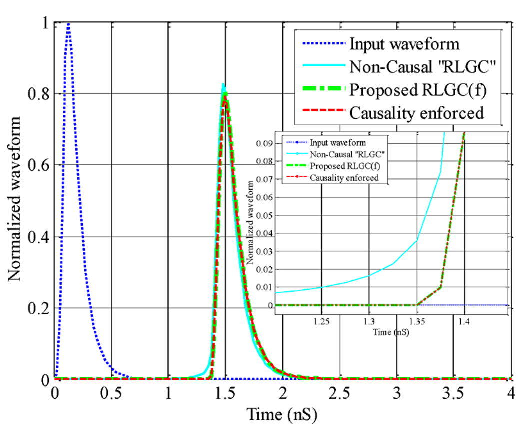

Fig. 4. Comparison of the time-domain waveforms at the receiving end for the single-ended stripline.

The second studied case is a single-ended microstrip transmission line. It is built on the top layer on a 26-layer board with FR-4 substrates. The cross-sectional dimensions of the microstrip and the test board are shown in Fig. 5, where $t = 2.4$ mil, $t1 = 1.35$ mil, $w = 5.75$ mil, and $h = 3.65$ mil. The microstrip is 6976 mil long after TRL calibration. S-parameters obtained from measurement, HSPICE simulation using the *RLGC*-I model with the extracted model parameters,

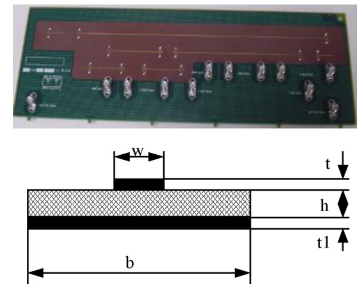

Fig. 5. Test board and the cross-sectional dimensions of the single-ended microstrip line.

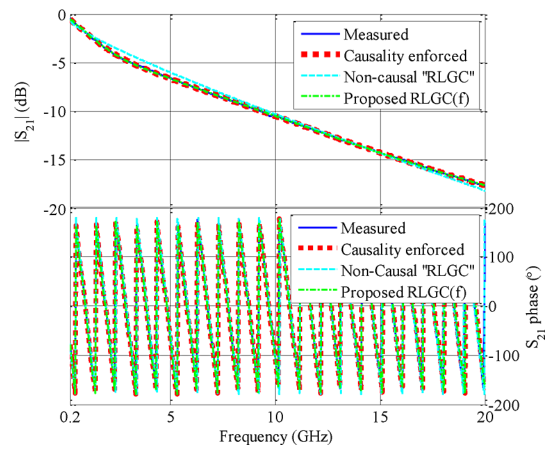

Fig. 6. S-parameter comparison between the *RLGC*(f) models (*RLGC*-I, II, and III) and the measurements for the microstrip line.

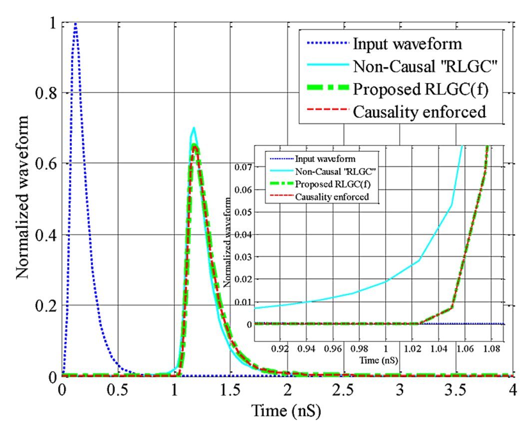

Fig. 7. Comparison of the time-domain waveforms at the receiving end for the microstrip line.

and the *RLGC*(f) model with two sets of model parameters extracted from the *RLGC*-II and *RLGC*-III models are compared in Fig. 6. The time-domain waveform comparison at the receiving end is shown in Fig. 7.

The third studied case is an edge-coupled differential stripline. It is built on layer 7 within an eight-layer board with FR-4 as substrates. The cross-sectional dimensions of the coupled stripline and the test board shown in Fig. 8 are $t = 1.35$ mil, $w = 10$ mil, and $s = 12.5$ mil. The coupled pair is 6905.5 mil long after TRL calibration [26]. Common-mode S-parameter

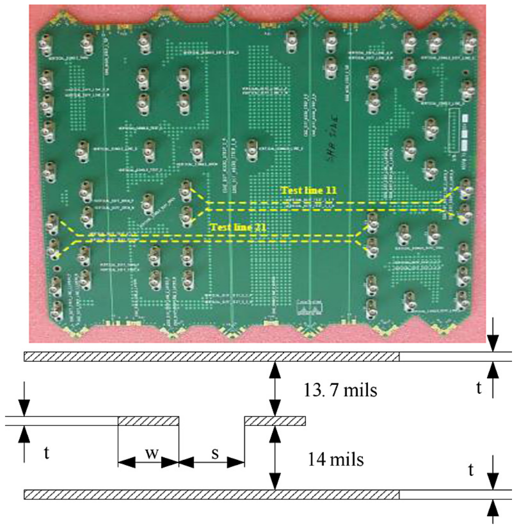

Fig. 8. Test board and the cross-sectional dimensions of the edge-coupled stripline.

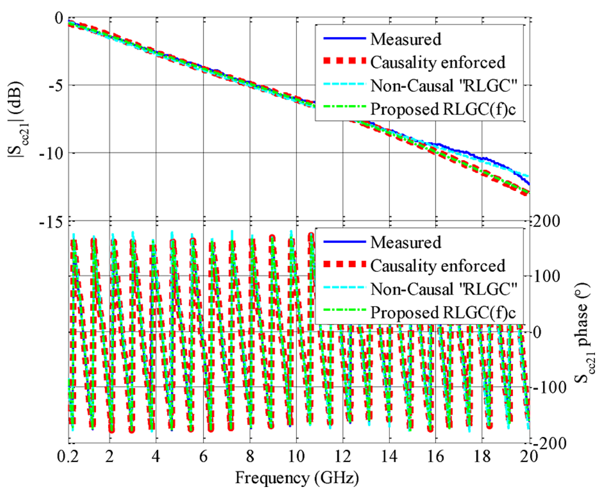

Fig. 9. Common-mode S-parameter comparison between the *RLGC*(f) models (*RLGC*-I, II, and III) and the measurements for the edge-coupled stripline.

comparison between the measurement and simulations using the *RLGC*-I model with extracted model parameters, and the *RLGC*(f) model with two sets of model parameters from the *RLGC*-II and the *RLGC*-III model extractions is shown in Fig. 9, while the differential-mode S-parameter comparison is shown in Fig. 10. The time-domain waveforms for the even mode and odd mode propagations through the stripline are shown in Figs. 11 and 12, respectively.

S-parameter comparisons, including the magnitude and the phase shown in Figs. 3, 6, 9, and 10, demonstrate that the proposed *RLGC*(f) model (*RLGC*-II), the analytical *RLGC* model (*RLGC*-I), and the causality enforced model (*RLGC*-III) agree well with the measurements. The maximum magnitude difference between simulation and measurement is less than 1 dB up to 20 GHz for the three studied cases, and the phase differences are hard to distinguish. However, the time-domain waveforms shown in Figs. 4, 7, 11, and 12 clearly demonstrate that the *RLGC*(f) models (*RLCG*-II and *RLCG*-III) are causal, but the *RLGC*-I model is not.

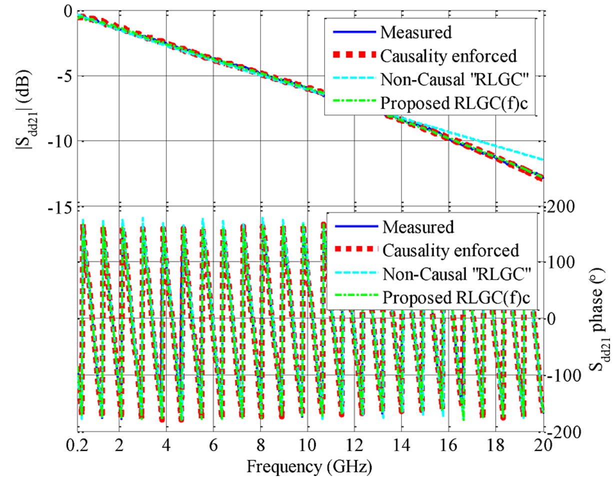

Fig. 10. Differential-mode S-parameter comparison between the *RLGC*(f) models (*RLGC*-I, II, and III) and the measurements for the edge-coupled stripline.

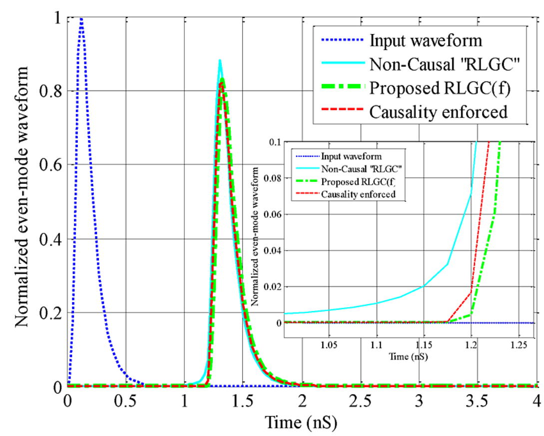

Fig. 11. Comparison of the time-domain even mode waveforms at the receiving end for the edge-coupled stripline.

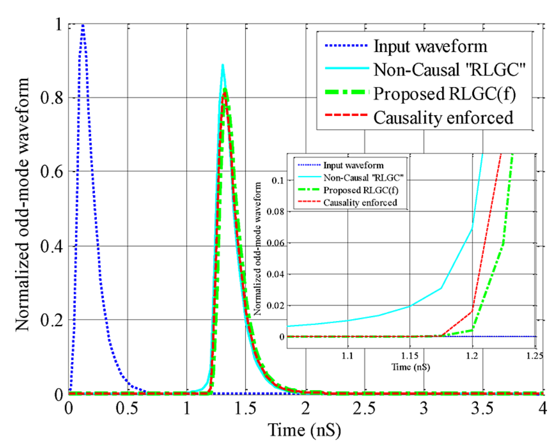

Fig. 12. Comparison of the time-domain odd mode waveforms at the receiving end for the edge-coupled stripline.

IV. Discussion and Conclusion

Frequency-dependent causal *RLGC*(f) models are proposed for single-ended and coupled transmission lines, and the methodology for building the models directly from measured S-parameters is developed. Time-domain waveforms in the three studied cases clearly show causal phenomena for the proposed *RLGC*(f) models while showing noncausal phenomena for the *RLGC*-I model. For the proposed *RLGC*(f) model, the start points of the received waveforms at the receiving end with model parameters extracted from S-parameters only (*RLGC*-II) and from the S-parameters plus enforced causality requirements (*RLGC*-III) are exactly same. This observation indicates that the proposed *RLGC*(f) model (*RLGC*-II) is causal, as expected. Therefore, enforcing the causality requirements in the model parameter extraction is not necessary.

Although the studied cases are tested on PCBs with FR-4-type epoxy resin fiber-glass-filled substrates in the frequency range from 200 MHz to 20 GHz, the approach presented herein is more general than that typically used to analyze PCBs. It can also be applied to on-silicon interconnects, provided that the TEM/quasi-TEM conditions are fulfilled for transmission lines, and causal relations for permittivity are valid for substrate dielectric materials. For higher frequency applications, or for modeling other types of substrate dielectric materials with more complex-shaped frequency dispersion, more than two Debye terms may be needed.

REFERENCES

[1] J. Zhang, M. Y. Koledintseva, J. L. Drewniak, D. J. Pommerenke, R. E. DuBroff, Z. Yang, W. Cheng, K. N. Rozanov, G. Antonini, and A. Orlandi, "Reconstruction of dielectric material parameters for dispersive substrate using a genetic algorithm," *IEEE Trans. Electromagn. Compat.*, vol. 50, no. 3, pp. 704–714, Aug. 2008.

[2] L. D. Landau and E. M. Lifshitz, *Electrodynamics of Continuous Media*. New York: Pergamon, 1960, pp. 239–312.

[3] S. L. Hahn, *Hilbert Transforms in Signal Processing*. Norwood, MA: Artech House, 1996.

[4] A. D. Poularikas, *The Transforms and Applications Handbook*. Boca Raton, FL: CRC Press, 1996, pp. 463–627.

[5] R. L. Wigington and N. S. Nahman, "Transient analysis of coaxial cables considering skin effect," in *Proc. IRE*, Feb., 1957, vol. 45, pp. 166–174.

[6] N. S. Nahman, "A discussion on the transient analysis of coaxial cables considering high-frequency losses," *IRE Trans. Circuit Theory*, vol. 9, pp. 144–152, Jun. 1962.

[7] D. R. Holt and N. S. Nahman, "Coaxial-line pulse-response error due to a planar skin-effect approximation," *IEEE Trans. Instrum. Meas.*, vol. IM-21, no. 4, pp. 515–519, Nov. 1972.

[8] N. S. Nahman and D. R. Holt, "Transient analysis of coaxial cables using skin effect approximation $A + B\sqrt{\mathrm{f}}$," *IEEE Trans. Circuit Theory*, vol. CT-19, no. 5, pp. 443–451, Sep. 1972.

[9] T. R. Arabi, A. T. Murphy, T. K. Sarkar, and R. F. Harrington, "On the modeling of conductor and substrate losses in multiconductor, multidielectric transmission line systems," *IEEE Trans. Microw. Theory Tech.*, vol. 39, no. 7, pp. 1090–1097, Jul. 1991.

[10] C. Svensson and G. E. Dermer, "Time domain modeling of lossy interconnects," *IEEE Trans. Adv. Packag.*, vol. 24, no. 2, pp. 191–196, May 2001.

[11] P. S. Neelakanta, *Handbook of Electromagnetic Materials—Monolithic and Composite Versions and Their Applications*. Boca Raton, FL: CRC Press, 1995, pp. 31–56.

[12] *Star-HSPICE Manual*, HSPICE, Fremont, CA, release 2001.2, Jun. 2001, ch.18.

[13] D. D. Pollock, *Physical Properties of Materials for Engineers*, 2nd ed. Boca Raton, FL: CRC Press, 1993, pp. 499–575.

[14] J. Zhang, M. Koledintseva, J. Drewniak, G. Antonini, A. Orlandi, and K. Rozanov, "Extracting R, L, G, C parameters of dispersive planar transmission lines from measured S-parameters using a genetic algorithm," in *Proc. 2004 IEEE Int. Symp. Electromagn. Compat.*, Santa Clara, CA, Aug., vol. 2, pp. 572–576.

[15] J. Zhang, M. Y. Koledintseva, R. E. DuBroff, D. J. Pommerenke, J. L. Drewniak, K. N. Rozanov, G. Antonini, and A. Orlandi, "Characterization of dispersive dielectrics using planar transmission line structures and genetic algorithm," submitted for publication.

[16] D. M. Pozar, *Microwave Engineering*, 2nd ed. New York: Wiley, 1998.

[17] R. Mongia, I. Bahl, and P. Bhartia, *RF and Microwave Coupled-Line Circuits*. Norwood, MA: Artech House, 1999, pp. 23–64.

[18] Y. Rahmat-Samii and E. Michielssen, *Electromagnetic Optimization by Genetic Algorithms*. New York: Wiley, 1999, pp. 1–93.

[19] L. Davis, *Handbook of Genetic Algorithms*. New York: Van Nostrand Reinhold, 1991, pp. 1–99.

[20] D. Quagliarella, J. Periaux, C. Poloni, and G. Winter, *Genetic Algorithms and Evolution Strategy in Engineering and Computer Science*. New York: Wiley, 1998, pp. 289–309.

[21] B. L. Miller and D. E. Goldberg, "Genetic algorithms, tournament selection, and the effects of noise," IlliGAL Rep. 95006, Jul. 1995.

[22] A. Papoulis, *The Fourier Integral and Its Applications*. New York: McGraw-Hill, 1962.

[23] S. K. Mitra, *Digital Signal Processing—A Computer-Based Approach*, 2nd ed. New York: McGraw-Hill, 2001, pp. 203–277.

[24] H. W. Bode, *Network Analysis and Feedback Amplifier Design*. New York: Van Nostrand, 1945.

[25] Agilent Technologies, "Agilent network analysis applying the 8510 TRL calibration for non-coaxial measurements," Agilent Technol., Santa Clara, CA, May 2001, Product Note 8510-8A.

[26] J. Zhang, Q. B. Chen, Z. Qiu, J. L. Drewniak, and A. Orlandi, "Using a single-ended TRL calibration pattern to de-embed coupled transmission lines," presented at the Int. Symp. Electromagn. Compat., Austin, TX, Aug. 17–21, 2009.

[27] IEC, "'Part 4-2: Testing and measurement techniques–Electrostatic discharge immunity test," unpublished.

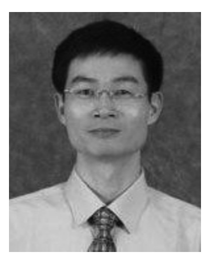

Jianmin Zhang (S'02–M'07–SM'09) received the B.S. degree from Southeast University, Nanjing, China, in 1985, and the M.S. and Ph.D. degrees in electrical engineering from the University of Missouri–Rolla, Rolla (renamed as Missouri University of Science and Technology in 2008), in 2003 and 2007, respectively.

During 1985, he was with the Nanjing Electronic Equipment Research Institute, China, as a Hardware Engineer. In 2007, he joined Cisco Systems, Inc., San Jose, CA, as a Senior Hardware Engineer, where he is involved in signal integrity and power integrity R&D for high-speed interconnects and design and analysis for high-performance networking products at the printed circuit board level, package level, and system level. His research interests include signal integrity, power integrity, SerDes modeling, and electromagnetic interference/electromagnetic compatibility for high-speed digital systems. He is the author or coauthor of more than 30 technical papers and is the inventor of three issued patents.

Dr. Zhang was the recipient of the Best Symposium Paper Award and the Best Student Symposium Paper Award from the IEEE Electromagnetic Compatibility Society in 2006, and the Conference Best Session Paper Award in signal integrity from the International Microelectronics and Packaging Society in 2007.

James L. Drewniak (S'85–M'90–SM'01–F'06) received the B.S., M.S., and Ph.D. degrees in electrical engineering from the University of Illinois, Urbana-Champaign, in 1985, 1987, and 1991, respectively.

In 1991, he joined the Electrical and Computer Engineering (ECE) Department, University of Missouri–Rolla, Rolla (renamed as Missouri University of Science and Technology in 2008), where he was the Director of the Materials Research Center during 2002–2007, and has been one of the Principal Investigators in the Electromagnetic Compatibility Laboratory and a Full Professor in the ECE Department. His research interests include electromagnetic compatibility (EMC) in high-speed digital and mixed-signal designs, electronic packaging, microelectromechanical systems, EMC in power-electronic-based systems, and numerical modeling for EMC applications.

David J. Pommerenke (M'98–SM'03) received the Ph.D. degree from the Technical University of Berlin, Berlin, Germany, in 1996.

He was with Hewlett Packard for five years. In 2001, he joined the Electromagnetic Compatibility Laboratory, University Missouri–Rolla, Rolla (renamed as the Missouri University of Science and Technology in 2008), where he is currently a Tenured Professor in the Electrical and Computer Engineering Department. Besides other professional activities, he is the U.S. representative of the Electrostatic Discharge (ESD) Standard Setting Group within the IEC TC77b. He was a Distinguished Lecturer for the IEEE Electromagnetic Compatibility (EMC) Society during 2006–2007. He is the author or coauthor of more than 100 papers and the Inventor of ten patents. His research interests include system-level ESD, numerical simulations, EMC measurement methods, and instrumentations.

Marina Y. Koledintseva (M'96–SM'03) received the M.S. (highest honors) and Ph.D. degrees from the Moscow Power Engineering Institute (Technical University)—MPEI (TU), Moscow, Russia, in 1984 and 1996, respectively.

During 1983–1999, she was a Researcher with the Ferrite Laboratory, MPEI (TU), where she was an Associate Professor from 1997 to 1999. In January 2000, she joined the Electromagnetic Compatibility (EMC) Laboratory, Missouri University of Science and Technology (MS&T), Rolla (known as the University of Missouri–Rolla before 2008), as a Visiting Professor, where she has been a Research Professor in the Electrical and Computer Engineering Department since 2005. Her current research interests include microwave engineering, interaction of electromagnetic fields with ferrites and composite media, their modeling, and application for electromagnetic compatibility. She is the author or coauthor of more than 150 papers. She is the holder of seven patents.

Dr. Koledintseva is a member of the Education, TC-9 Computational Electromagnetics, and TC-11 (Nanotechnology) Committees of the IEEE Electromagnetic Compatibility Society.

Richard E. DuBroff (S'74–M'77–SM'84) received the B.S.E.E. degree from Rensselaer Polytechnic Institute, Troy, NY, in 1970, and the M.S. and Ph.D. degrees in electrical engineering from the University of Illinois, Urbana-Champaign, in 1972 and 1976, respectively.

From 1976 to 1978, he was a Postdoctoral Researcher with the Ionosphere Radio Laboratory, University of Illinois, Urbana-Champaign, where he was involved with backscatter inversion of ionospheric electron density profiles. From 1978 to 1984, he was a Research Engineer in the Geophysics Branch of Phillips Petroleum, Bartlesville, OK. Since 1984, he has been with the University of Missouri, Rolla (renamed as the Missouri University of Science and Technology in 2008), where he was an Associate Chairman for graduate studies from 1991 to 1996 and from 2002 to 2009, and is currently a Professor in the Electrical and Computer Engineering Department.

Wheling Cheng received the Bachelor's degree from Chiao-Tung University, Hsinchu, Taiwan, in 1986, and the Ph.D. degree from Stanford University, Stanford, CA, in 1995.

During 1995–1997, she was with nChip, where she was involved in multichip module development and fabrication. During 1997–1999, she was with LSI Logic, where she was involved with signal integrity analysis and package design. From 1999 to July 2009, she was with Cisco Systems, Inc., where she was engaged in signal integrity and power integrity analysis. In August 2009, she joined Juniper Networks, Sunnyvale, CA, as a member of the Technical Staff. Her current research interests include 3-D modeling of high-speed interconnects and SerDes channel analysis.

Zhiping Yang (S'97–M'00–SM'05) received the B.S. and M.S. degrees from Tsinghua University, Beijing, China, in 1994 and 1997, respectively, and the Ph.D. degree from the University of Missouri-Rolla, Rolla (renamed as the Missouri University of Science and Technology in 2008), in 2000.

He was a Principal Signal Integrity Engineer with Apple Computer. He was a Technical Leader with Cisco System, Inc., San Jose, CA, where he is currently a Senior Manager of Hardware Engineering. He was a member of the Technical Staff with Nuova Systems, Inc. His research interests include signal integrity and power integrity methodology development for die/package/board codesign, application of embedded passives, extraction of material properties at high frequency, and high-speed differential signaling technology. He is actively involved with I/O buffer information spec (IBIS) standard activities. His research in power integrity greatly increases IBIS model's simulation accuracy under nonideal power supply conditions. In 2005, the IBIS Standard Committee ratified BIRD95.6 proposal, which was coauthored by him and his colleagues in Cisco Systems and Teraspeed Consulting Group. He is the author or coauthor of more than 20 research papers. He holds six issued and two pending U.S. patents.

Qinghua B. Chen (S'95–M'96) received the B.S.E.E. and M.S.E.E. degrees from Tsinghua University, Beijing, China, and the Ph.D. degree from Texas A&M University, College Station.

He worked with Andiamo Systems, Inc., as a Manager and a Technical Leader, where he was in charge of high-speed signal integrity activities. He was also with Raza Foundries, Inc., Nplab, Inc., and Texas Instruments, Inc., as a Technical Leader/ Senior Design Engineer, where he was engaged in high-speed IC/system designs. He is currently a Senior Engineering Manager with Cisco Systems, Inc., San Jose, CA, where he is engaged with high-speed high-performance networking product R&D.

Antonio Orlandi (M'90–SM'97–F'07) was born in Milan, Italy, in 1963. He received the Laurea degree in electrical engineering from the University of Rome "La Sapienza," Rome, Italy, in 1988.

From 1988 to 1990, he was with the Department of Electrical Engineering, University of Rome "La Sapienza." Since 1990, he has been with the Department of Electrical Engineering, University of L'Aquila, L'Aquila, Italy, where he is currently a Full Professor and the Chair of the UAq Electromagnetic Compatibility (EMC) Laboratory. He is the author or coauthor of more than 200 technical papers published in the field of EMC in lightning protection systems and power drive systems. His research interests include numerical methods and modeling techniques to approach signal/power integrity, and EMC/electromagnetic interference issues in high-speed digital systems.

Dr. Orlandi is a member of the Education, TC-9 Computational Electromagnetics, and the Chairman of the TC-10 "Signal Integrity" Committees of the IEEE EMC Society. He was the recipient of the IEEE TRANSACTIONS ON ELECTROMAGNETIC COMPATIBILITY Best Paper Award in 1997, the IEEE EMC Society Technical Achievement Award in 2003, the IBM Shared University Research Award in 2004–2006, the Computer Simulation Technology University Award in 2004, and the IEEE International Symposium on EMC Best Paper Award in 2009. He was an Associate Editor of the IEEE TRANSACTIONS ON ELECTROMAGNETIC COMPATIBILITY from 1996 to 2000 and the IEEE TRANSACTIONS ON MOBILE COMPUTING from 2001 to 2006, and has been the Symposium Chairman of the TC-5 "Signal Integrity" Technical Committee of the International Zurich Symposium and Technical Exhibition on EMC since 1999.